LAWRENCE
LIVERMORE
NATIONAL
LABORATORY

LLNL-JRNL-409957

Elimination of instrumental asymmetries in spin resolved photoemission with unpolarized light

S.-W. Yu, B. W. Chung, J. G. Tobin, T. Komesu, G. D. Waddill

January 20, 2009

Nuclear Instruments and Methods in Physics Research A

Disclaimer

Elimination of instrumental asymmetries in spin resolved photoemission with unpolarized light

S.-W. Yu,[1,*] B. W. Chung,[1] J. G. Tobin,[1] Takashi Komesu,[2,†] and G.D. Waddill[2]

[1]*Lawrence Livermore National Laboratory, Livermore, CA*

[2]*Missouri University of Science and Technology, Physics Department, Rolla, MO*

Abstract

We introduce a new method to eliminate instrumental asymmetries in spin resolved photoemission with excitation by unpolarized light. The new method is applied successfully to analyze the spin polarizations in the valence band and $4d$ core level photoemission, excited with unpolarized light from a nonmagnetic Pt crystal. It is also applied to the spin analysis of the $2p$ core level photoemission, generated with circularly polarized x-rays from magnetic Fe. We argue that this new method can be used for spin analysis in spin resolved photoemission, with both unpolarized (linearly polarized) light and circularly polarized light from nonmagnetic and magnetic materials.

PACS numbers:

*Corresponding Author: YU21@LLNL.GOV

†Present address: Spring8, Japan

I. INTRODUCTION

In photoemission investigations of magnetic and nonmagnetic materials, the measurement of the electron spin polarization with respect to a suitably chosen quantization direction can provide new insight into the electronic structure of the systems under study, which cannot be gleaned from the energy and momentum relationship of the photoelectrons [1–3]. The most common method for the electron spin polarization is the measurement of the left-right scattering asymmetry of an electron beam with spin polarization normal to the scattering plane [4–9]. This left-right scattering asymmetry based on Mott scattering is characterized by an asymmetry A defined by

$$A = \frac{N_{\mathrm{L}} - N_{\mathrm{R}}}{N_{\mathrm{L}} + N_{\mathrm{R}}}, \tag{1}$$

where N_{L} and N_{R} are the numbers of electrons scattered to the left and the right, respectively. From this asymmetry A, one can determine the spin polarization P by

$$P = \frac{1}{S_{\mathrm{eff}}} A, \tag{2}$$

if the effective Sherman function S_{eff}, which represents the sensitivity of the target, is known. From Eq. (2), it is clear that the accurate measurement of the asymmetry A, with the accurate knowledge of S_{eff} results in the accurate spin polarization P. In the real measurements of the spin polarization, however, the asymmetry A measured contains not only the asymmetry induced by the physical events, but also the instrumental asymmetry originating from the experimental errors. Experimental evidence indicates strongly that the instrumental asymmetry depends not only on the energy of the electron, but also on time. If S_{eff} is well known, in fact, the accuracy of experimental data is limited not only by statistics, but also by the uncertainty in elimination of the instrumental asymmetry.

In spin resolved photoemission experiments with circularly polarized light, the instrumental asymmetry can be eliminated using the two helicities of the circularly polarized light, under the condition that the instrumental asymmetry does not change over time. Due to the symmetry, the flipping of the helicity results in the reverse of the spin polarization while leaving the instrumental asymmetry unchanged [10, 11]. (This helicity flipping is completely analogous to that traditionally done in spin resolved spectroscopy, where magnetization flipping reverses the spin polarization while leaving the instrumental asymmetry as is). It is especially crucial to eliminate the instrumental asymmetry quantitatively if one works with

unpolarized (or linearly polarized) light in which the helicity of the light, and therefore the spin polarization cannot be reversed [11]. Therefore, our goal in this paper is to introduce a new method to eliminate the instrumental asymmetries in the spin resolved photoemission when unpolarized light is used.

II. OVERVIEW OF SPIN RESOLVED PHOTOEMISSION WITH UNPOLARIZED LIGHT

Fig. 1 illustrates an overview of the spin resolved photoemission system with unpolarized light installed at the Lawrence Livermore National Laboratory [12, 13]. As the photon sources, there are two unpolarized ultraviolet lights (UV1 and UV2) located in X-Z plane at an angle of 45° and −45° with respect to the surface normal of the sample, respectively, and an unpolarized x-ray source (Mg $K\alpha$ and Al $K\alpha$) located in Y-Z plane at an angle of 45° with respect to the surface normal of the sample. The advantage of the two UV sources is that they provide a possibility to remove the instrumental asymmetry as will be shown in section IV. The energies of the photoelectrons are analyzed by the hemispherical electron energy analyzer. The electrons in the central part of the exit plane are directed through an aperture into the acceleration lens. The electrons accelerated through the acceleration lens hit a Thorium target at 25 kV for their spin analysis. The electrons scatter from the target and after being decelerated to almost ground potential, they are detected by 4 channeltrons in the Mott detector. In the Mott detector, the two transversal spin components P_X and P_Y are determined simultaneously [4, 5].

III. MOTT SCATTERING

The physical principal of Mott detection is based on the left-right scattering asymmetry caused by the spin-orbit interaction in the electron-atom scattering [4, 5]. Consider a scattering of a high energy electron by a nucleus of charge Ze. The motion of the electron in the electric field $\mathbf{E}$ of the nucleus results in a magnetic field $\mathbf{B}$ in the electron rest frame induced by the Lorentz transformation of the electric field. The interaction between the magnetic field $\mathbf{B}$ and the electron spin magnetic moment creates an additional spin-orbit term $V_{\rm so}$ in the scattering potential. The presence of the spin-orbit term $V_{\rm so}$ in the scattering potential

introduces a spin dependence in the scattering cross section which can be written

$$\sigma(\theta, \phi) = I(\theta)[1 + S_{\text{eff}}(\theta)\mathbf{P} \cdot \hat{\mathbf{n}}], \tag{3}$$

where $I(\theta)$ is the intensity without the spin-orbit term V_{so}, $\mathbf{P}$ is the polarization vector of the incident electron beam, $\hat{\mathbf{n}}$ is the unit vector normal to the scattering plane defined by the momentum of the incident electrons and the momentum of the scattered electrons in the following $\hat{\mathbf{n}} = \frac{\mathbf{k}\times\mathbf{k}'}{|\mathbf{k}\times\mathbf{k}'|}$. The Eq. (3), which is independent of the choice of coordinate system because the scalar product is invariant under coordinate transformations, is the basic equation for the measurement of the spin polarization by Mott scattering. An essential feature of Eq. (3) is that only the component of the polarization vector perpendicular to the scattering plane contributes to the scattering asymmetry while components parallel to the scattering plane make no contribution. Therefore, as shown in Figs. 1 and 2, spin component P_Y can be measured by counters 3 and 4 (not counters 1 and 2) while spin component P_X can be measured by counters 1 and 2. Another point to be mentioned about Eq. (3) is that for a given spin polarization, $\mathbf{P} \cdot \hat{\mathbf{n}}$ is always a positive value for the left counter and a negative value for the right counter. For example, for $P_Y(P_X)$, $\mathbf{P} \cdot \hat{\mathbf{n}}$ is always positive value for the left counter 3(1) and negative value for the right counter 4(2) in Figs. 1 and 2. Therefore, Mott scattering is always called to be based on "left-right" scattering asymmetry (not "right-left"). Fig. 3 shows the azimuthal angle (ϕ) dependency of the scattering cross section $\sigma(\theta, \phi)$ according to the Eq. (3). It is worth noting that there would be no azimuthal angle dependency of the scattering cross section if the effective Sherman function $S_{\text{eff}}(\theta)$ becomes zero. For example, $S_{\text{eff}}(\theta)$ approaches zero under the small scattering angle θ [5].

IV. DETERMINATION OF ELECTRON SPIN POLARIZATION

It is an essential task to determine the spin polarization with the Mott detector. In order to illustrate how the spin polarization can be determined with the Mott detector, the counting rates at the counters 1, 2, 3, and 4 located in the back scattering direction as shown in Fig. 1 are denoted as N_1, N_2, N_3, and N_4 . For P_Y (P_X) component, the counter 3 (counter 1) is in the left side and the counter 4 (counter 2) is in the right side. As the physical principle of Mott detection is based on the left-right scattering asymmetry caused

by the spin-orbit interaction, in principle, the different counting rates between N_3 and N_4(N_1 and N_2) allow to evaluate the spin polarization $P_Y(P_X)$, according to the Eqs. (1) and (2), provided that the S_{eff} is known.

However, in real experiments, the experimental setup usually involves instrumental asymmetries. The instrumental asymmetries are caused by: (i) different counter efficiencies, e.g. given by different solid angles accepted by the counters or different windows of the counters; and (ii) misalignment of the incident beam, e.g. parallel shift or oblique incidence with respect to the ideal axis (called false asymmetries) [10, 11]. These instrumental asymmetries have to be eliminated, otherwise the measured spin polarization cannot be claimed to be accurate. Indeed, elimination of these instrumental asymmetries is not easy, especially when unpolarized (linearly polarized) light as excitation source is used. In the following subsections it will be described how the instrumental asymmetries can be eliminated in the measurements with unpolarized light.

A. Circularly polarized radiation

The main purpose of this publication is to demonstrate how the instrumental asymmetries can be eliminated when unpolarized light is used as excitation source. But let us digress to show the case with circularly polarized light first. The instrumental asymmetries indicated above can be eliminated completely by using circularly polarized light (σ^+, σ^-) [11]. Let us use our experimental setup at the Advanced Photon Source (APS) as shown in Fig. 4 to explain the case [14–16]. Circularly polarized light from the APS hits the sample and furthermore we assume that we measure the spin component P_Z by using counters 1 and 2 in Fig. 4. The experimental setup shown in Fig. 4 is basically identical to the experimental setup shown in Fig. 1, except for that Fig. 4 has a 90° deflector. The role of the 90° deflector is to transfer a longitudinal polarization component to a transversal polarization component as shown in inset of Fig. 4. Before the deflector, the spin polarized electron beam moves along Z-direction with a longitudinal component P_Z and the two transversal components P_X and P_Y. When the spin polarized electron beam is deflected by 90° in an electrostatic field, the velocity of the spin polarized electron beam is changed from Z-direction to X-direction, but its spin components are kept unchanged in the nonrelativistic approximation, so that the P_Z becomes transverse and P_X becomes longitudinal. Therefore, the spin component P_Z

can be measured in Mott detector since only two transversal components can be measured in Mott detector. The spin component P_Z cannot be measured in the experimental setup shown in Fig. 1 because P_Z is a longitudinal component in Fig. 1.

Circularly polarized light creates a spin component which is aligned along the photon propagation direction [5]. This means that if circularly polarized light lying in the X-Z plane in Fig. 4 hits the sample, it can create a spin component P_Z. Denoting the efficiencies of the counters 1 and 2 by W_1 and W_2, respectively, for σ^+ light, one measures the intensities in the Mott detector [11]:

$$N_1(\sigma^+) \sim W_1(1 + P_Z S_{\text{eff}})(1 + A_f), \tag{4}$$

$$N_2(\sigma^+) \sim W_2(1 - P_Z S_{\text{eff}})(1 - A_f), \tag{5}$$

where A_f denote the false asymmetry caused by instrumental misalignments. By changing the helicity from σ^+ to σ^-, only the spin polarization is reversed and it follows,

$$N_1(\sigma^-) \sim W_1(1 - P_Z S_{\text{eff}})(1 + A_f), \tag{6}$$

$$N_2(\sigma^-) \sim W_2(1 + P_Z S_{\text{eff}})(1 - A_f). \tag{7}$$

From the Eqs. (4-7) one obtains the following relation

$$\begin{aligned} Q &\equiv \sqrt{\left(\frac{N_1(\sigma^+)}{N_2(\sigma^+)} \Big/ \frac{N_1(\sigma^-)}{N_2(\sigma^-)}\right)} \\ &= \sqrt{\left(\frac{W_1}{W_2}\right)\left(\frac{1 + P_Z S_{\text{eff}}}{1 - P_Z S_{\text{eff}}}\right)\left(\frac{1 + A_f}{1 - A_f}\right)\left(\frac{W_2}{W_1}\right)\left(\frac{1 + P_Z S_{\text{eff}}}{1 - P_Z S_{\text{eff}}}\right)\left(\frac{1 - A_f}{1 + A_f}\right)} \\ &= \frac{1 + P_Z S_{\text{eff}}}{1 - P_Z S_{\text{eff}}}. \end{aligned} \tag{8}$$

Eq. 8 shows that the counter efficiencies W_1 and W_2 as well as the false asymmetry A_f are completely eliminated. Therefore, the spin polarization P_Z can be calculated from the counting rates $N_1(\sigma^{\pm})$ and $N_2(\sigma^{\pm})$ by

$$P_Z = \frac{1}{S_{\text{eff}}}\left(\frac{Q - 1}{Q + 1}\right) = \frac{1}{S_{\text{eff}}}\left(\frac{\sqrt{N_1(\sigma^+)N_2(\sigma^-)} - \sqrt{N_2(\sigma^+)N_1(\sigma^-)}}{\sqrt{N_1(\sigma^+)N_2(\sigma^-)} + \sqrt{N_2(\sigma^+)N_1(\sigma^-)}}\right). \tag{9}$$

It is very important to note that in order to determine the spin polarization P_Z using the Eq. (9), the instrumental asymmetry A_Z^{ins} defined in the following way

$$A_Z^{\text{ins}} = \frac{\sqrt{N_1(\sigma^+)N_1(\sigma^-)}}{\sqrt{N_2(\sigma^+)N_2(\sigma^-)}} \tag{10}$$

has to be monitored for every run [5]. If $A_Z^{\rm ins}$ differs from 1, this means that there is an instrumental asymmetry. The instrumental asymmetry can be eliminated by using the Eq. (9) only if $A_Z^{\rm ins}$ does not vary in time [5]. Therefore, monitoring of $A_Z^{\rm ins}$ provides an important check on the performance of the Mott detector. If $A_Z^{\rm ins}$ is not constant over runs, the spin polarization determined by using Eq. (9) cannot be claimed to be accurate.

In order to illustrate the situation clearly, the spin resolved photoelectron spectra from Ce $3d_{5/2}$ measured with the experimental setup shown in Fig. 4 with circularly polarized light of hν=1350 eV are presented in Fig. 5. It should be mentioned that since this paper aims to describe the technical method to determine the spin polarization using Mott detector, the physical mechanism for the spin polarization is discussed in another publication [14]. Fig. 5 contains the three independent measurements collected in sequence (Sets 1,2,3). For example, for Set 1: with σ^+, the kinetic energies of the $3d_{5/2}$ photoelectrons are scanned, which produced $N_1(\sigma^+)$ and $N_2(\sigma^+)$. After that, with σ^-, the identical kinetic energies are scanned, which produces $N_1(\sigma^-)$ and $N_2(\sigma^-)$. Then using Eqs. (9) and (10), the spin polarization P_Z and the instrumental asymmetry $A_Z^{\rm ins}$ are calculated and shown in middle and bottom panels, respectively, of Fig. 5. The spin-separated partial intensities for spin parallel I_+ and antiparallel I_- to the photon propagation direction are derived from the spin integrated total intensity I (I=$N_1(\sigma^+)$ + $N_2(\sigma^+)$ + $N_1(\sigma^-)$ + $N_2(\sigma^-)$) and the spin polarization P_Z using $I_\pm = (I/2)(1 \pm P_Z)$, and they are shown in the top panels of Fig. 5.

In order to compare the instrumental asymmetries and the spin polarizations carefully, the instrumental asymmetries and the spin polarizations from the three Sets of Fig. 5 are overlapped in Fig. 6. By co-plotting the instrumental asymmetries for the three Sets, we notice that there are instrumental asymmetries because $A_Z^{\rm ins}$ differ from 1 for the all three Sets. Furthermore, $A_Z^{\rm ins}$ overlaps well for Sets 1 and 2 within the statistical error bars while $A_Z^{\rm ins}$ from Set 3 deviates significantly from the Sets 1 and 2. What this means is that there is an instrumental asymmetry which keeps constant during the measurements for Sets 1 and 2, but it is changed during the measurement for Set 3. As mentioned above, if $A_Z^{\rm ins}$ changes during the measurement, the consequence is that it causes a wrong polarization. A clear example for such wrong polarization is the large spin polarizations at the outsides of the peak as indicated as arrows in Set 3 of Fig. 5. In principle, the spin polarization is supposed to be zero at the outsides of the peak because there is no physical mechanism to be spin polarized for nonmagnetic materials. As a result, Set 3 cannot be used to determine the

spin polarization. Only Sets 1 and 2 may be used.

In general, instrumental asymmetry changes with time. Therefore, it would be wise to measure a Set as short as reasonably possible, so that the Set can be completed before instrumental asymmetry changes. Through this way, many Sets should be accumulated to improve the statistics and confirm the consistency of each measurement.

From the law of error propagation, the single statistical errors for ΔP_Z and $\Delta A_Z^{\rm ins}$ can be expressed in terms of $N_1(\sigma^{\pm})$ and $N_2(\sigma^{\pm})$ by

$$\begin{aligned}
\Delta P_Z &= \sqrt{\sum_{\sigma^{\pm}}\left(\frac{\partial P_Z}{\partial N_1(\sigma^{\pm})}\right)^2(\Delta N_1(\sigma^{\pm}))^2+\sum_{\sigma^{\pm}}\left(\frac{\partial P_Z}{\partial N_2(\sigma^{\pm})}\right)^2(\Delta N_2(\sigma^{\pm}))^2} \\
&= \frac{1}{S_{\rm eff}}\sqrt{\frac{4\sqrt{N_1(\sigma^+)N_2(\sigma^-)}\sqrt{N_2(\sigma^+)N_1(\sigma^-)}}{\left(\sqrt{N_1(\sigma^+)N_2(\sigma^-)}+\sqrt{N_2(\sigma^+)N_1(\sigma^-)}\right)^3}}, \\
\Delta A_Z^{\rm ins} &= \sqrt{\sum_{\sigma^{\pm}}\left(\frac{\partial A_Z^{\rm ins}}{\partial N_1(\sigma^{\pm})}\right)^2(\Delta N_1(\sigma^{\pm}))^2+\sum_{\sigma^{\pm}}\left(\frac{\partial A_Z^{\rm ins}}{\partial N_2(\sigma^{\pm})}\right)^2(\Delta N_2(\sigma^{\pm}))^2} \\
&= \frac{1}{2}A_Z^{\rm ins}\sqrt{\sum_{\sigma^{\pm}}\left(\frac{1}{N_1(\sigma^{\pm})}\right)+\sum_{\sigma^{\pm}}\left(\frac{1}{N_2(\sigma^{\pm})}\right)}.
\end{aligned} \tag{11}$$

For the errors $\Delta N_i(\sigma^{\pm})$ of the individual measurements, the statistical errors $\sqrt{N_i(\sigma^{\pm})}$ have been substituted. These equations have been used to produce the error bars in Figs. 5 and 6.

B. Unpolarized light

It is especially difficult to eliminate the instrumental asymmetries quantitatively if one works with linearly polarized or unpolarized light in which the helicity of light, and therefore the spin polarization cannot be reversed completely [11]. However, as will be shown in this subsection, we introduce a new method to eliminate the instrumental asymmetries.

Let us assume that unpolarized light from the UV1 shown in Fig. 1 hits the sample, and that we measure the spin component P_Y. The counting rates $N_3(\mathrm{un})$, $N_4(\mathrm{un})$ of the back scattering counters 3 and 4 are given by [11]

$$N_3(\mathrm{un}) \sim W_3(1+P_Y S_{\rm eff})(1+A_f), \tag{12}$$

$$N_4(\mathrm{un}) \sim W_4(1-P_Y S_{\rm eff})(1-A_f). \tag{13}$$

Now, let us consider the case where $P_Y = 0$, i.e., there is no spin polarization due to the real physical event. If the counting rates for $P_Y = 0$ are denoted by $N_3^0(\mathrm{un})$ and $N_4^0(\mathrm{un})$, respectively, the Eqs. (12) and (13) can be written

$$N_3^0(\mathrm{un}) \sim W_3(1 + A_f), \tag{14}$$

$$N_4^0(\mathrm{un}) \sim W_4(1 - A_f). \tag{15}$$

From Eqs. (14) and (15), the pure instrumental asymmetry A_Y^0 for $P_Y = 0$ is defined by

$$A_Y^0 \equiv \frac{N_3^0(\mathrm{un}) - \mathrm{N}_4^0(\mathrm{un})}{N_3^0(\mathrm{un}) + \mathrm{N}_4^0(\mathrm{un})} = \frac{W_3(1 + A_f) - W_4(1 - A_f)}{W_3(1 + A_f) + W_4(1 - A_f)}. \tag{16}$$

Now, using Eqs. (12-16) we define the asymmetry A_Y which includes both the pure instrumental asymmetry A_Y^0 and the asymmetry caused by the real physical spin polarization

$$\begin{aligned} A_Y &\equiv \frac{N_3(\mathrm{un}) - \mathrm{N}_4(\mathrm{un})}{N_3(\mathrm{un}) + \mathrm{N}_4(\mathrm{un})} \\ &= \frac{W_3(1 + A_f)(1 + P_Y S_{\mathrm{eff}}) - W_4(1 - A_f)(1 - P_Y S_{\mathrm{eff}})}{W_3(1 + A_f)(1 + P_Y S_{\mathrm{eff}}) + W_4(1 - A_f)(1 - P_Y S_{\mathrm{eff}})} \\ &= \frac{\Big(W_3(1 + A_f) - W_4(1 - A_f)\Big) + \Big((W_3(1 + A_f) + W_4(1 - A_f)\Big) P_Y S_{\mathrm{eff}}}{\Big(W_3(1 + A_f) + W_4(1 - A_f)\Big) + \Big(W_3(1 + A_f) - W_4(1 - A_f)\Big) P_Y S_{\mathrm{eff}}} \\ &= \frac{A_Y^0 + P_Y S_{\mathrm{eff}}}{1 + A_Y^0 P_Y S_{\mathrm{eff}}}. \end{aligned} \tag{17}$$

Therefore, from Eq. (17) the spin polarization P_Y can be written

$$P_Y = \frac{1}{S_{\mathrm{eff}}} \left(\frac{A_Y - A_Y^0}{1 - A_Y A_Y^0} \right). \tag{18}$$

The Eq. (18) indicates that the spin polarization P_Y can be determined by means of the counting rates $N_3(\mathrm{un})$ and $N_4(\mathrm{un})$ given by Eqs. (12) and (13) if the pure instrumental asymmetry A_Y^0 is known.

In order to explain how the Eq. (18) works, the spin resolved photoemission spectra obtained with unpolarized UV1 and UV2 from the valence-bands of Pt(001) are presented in Fig. 7(b) and (c), respectively. In the bottom panel of Fig. 7(b), the asymmetry A_Y, which contains the pure instrumental asymmetry A_Y^0 and the real physical asymmetry, is plotted as a function of the binding energy. To use Eq. (18), we have to assume the pure instrumental asymmetry A_Y^0 behaves in a reasonable way. First, we assume that the A_Y^0

does not vary in time. Second, we assume that the spin polarization should be zero at the outsides of the peak and at the between peaks because there is no physical mechanism for nonzero spin polarization in nonmagnetic materials. Based on these assumptions, a reasonable A_Y^0 is assumed as a line shown in the bottom panel of Fig. 7(b). If we know the pure instrumental asymmetry A_Y^0, the spin polarization P_Y can be calculated with Eq. (18) as shown in the middle panel of Fig. 7(b). Fig. 7 (c) shows the spin resolved photoemission spectra obtained with UV2. Since UV2 is symmetric to UV1 along Z-direction, the spin polarization measured with UV2 should be identical to the one measured with UV1, except for that the sign of the spin polarization is reversed. Similarly to the measurement with UV1, the pure instrumental asymmetry A_Y^0 is assumed as a line shown in the bottom panel of Fig. 7 (c), and then the spin polarization is calculated using Eq. (18) as shown in the middle panel of Fig. 7 (c). Comparison between the measurements with UV1 and UV2 shows identical polarization within the error bars, with reversed sign.

Fig. 8 shows spin resolved photoemission spectra excited with unpolarized x-rays (hν=1253.6 eV) from the $4d_{5/2}$ and $4d_{3/2}$ core levels of Pt(001), for the two spin components P_X and P_Y. As shown in Fig. 1, the x-ray tube is located in the Y-Z plane at an angle of 45° with respect to the surface normal. By the symmetry reason, the spin component P_X, which is perpendicular to the reaction plane defined by the incident photons and the outgoing electrons, is spin polarized while P_Y, which is parallel to the reaction plane, is unpolarized [12, 13]. Let us consider the P_X component first. The asymmetry A_X is plotted in the bottom panel of Fig. 8 (a). In order to determine the spin polarization P_X using Eq. (18), the pure instrumental asymmetry A_X^0 is assumed as a line shown in the bottom panel of Fig. 8 (a). Here, also the two conditions are assumed that the A_Y^0 does not vary in time, and that the spin polarization should be zero at the outsides of the peak and at the between peaks. The middle panel of Fig. 8 (a) shows the resulting spin polarization P_X. Similarly, the spin polarization P_Y is determined and shown in Fig. 8 (b).

From the above examples, it is clear that the Eq. (18) is a useful way to determine the spin polarizations in the spin resolved photoemission with unpolarized light which does not have two helicities.

Considering that we have developed a format for a helicity flip that is analogous to a magnetization flip in magnetic systems, it is reasonable to inquire whether a format for a geometry flip with unpolarized light would also be feasible. Since there are two photon

sources (UV1 and UV2), which are in symmetry along the Z-direction as shown in Fig. 1, the following method is also possible. With UV1, the counting rates N_3(UV1) and N_4(UV1) can be written

$$N_3(\mathrm{UV1}) \sim W_3(1 + P_Y S_{\mathrm{eff}})(1 + A_f), \tag{19}$$

$$N_4(\mathrm{UV1}) \sim W_4(1 - P_Y S_{\mathrm{eff}})(1 - A_f). \tag{20}$$

With UV2, since only spin polarization is reversed, the counting rates N_3(UV2) and N_4(UV2) can be written

$$N_3(\mathrm{UV2}) \sim W_3(1 - P_Y S_{\mathrm{eff}})(1 + A_f), \tag{21}$$

$$N_4(\mathrm{UV2}) \sim W_4(1 + P_Y S_{\mathrm{eff}})(1 - A_f). \tag{22}$$

From the Eqs. (19-22) one obtains the following relation

$$\begin{aligned} R &\equiv \sqrt{\left(\frac{N_3(\mathrm{UV1})}{N_4(\mathrm{UV1})}\Big/\frac{N_3(\mathrm{UV2})}{N_4(\mathrm{UV2})}\right)} \\ &= \sqrt{\left(\frac{W_3}{W_4}\right)\left(\frac{1+P_Y S_{\mathrm{eff}}}{1-P_Y S_{\mathrm{eff}}}\right)\left(\frac{1+A_f}{1-A_f}\right)\left(\frac{W_4}{W_3}\right)\left(\frac{1+P_Y S_{\mathrm{eff}}}{1-P_Y S_{\mathrm{eff}}}\right)\left(\frac{1-A_f}{1+A_f}\right)} \\ &= \frac{1+P_Y S_{\mathrm{eff}}}{1-P_Y S_{\mathrm{eff}}}. \end{aligned} \tag{23}$$

Therefore, from Eq. (23)

$$P_Y = \frac{1}{S_{\mathrm{eff}}}\left(\frac{R-1}{R+1}\right) = \frac{1}{S_{\mathrm{eff}}}\left(\frac{\sqrt{N_3(\mathrm{UV1})\mathrm{N}_4(\mathrm{UV2})} - \sqrt{N_4(\mathrm{UV1})\mathrm{N}_3(\mathrm{UV2})}}{\sqrt{N_3(\mathrm{UV1})\mathrm{N}_4(\mathrm{UV2})} + \sqrt{N_4(\mathrm{UV1})\mathrm{N}_3(\mathrm{UV2})}}\right). \tag{24}$$

Analogue to Eq. (10), the instrumental asymmetry A_Y^{ins} can be defined

$$A_Y^{\mathrm{ins}} = \frac{\sqrt{N_3(\mathrm{UV1})\mathrm{N}_3(\mathrm{UV2})}}{\sqrt{N_4(\mathrm{UV1})\mathrm{N}_4(\mathrm{UV2})}}. \tag{25}$$

The Fig. 7 (a) illustrates the spin polarization P_Y determined by using the Eq. (24) with the counting rates N_3(UV1), N_4(UV1), N_3(UV2), and N_4(UV2). The spin polarizations determined by Eq. (18) and Eq. (24) are identical within the statistics of the experiment.

The bottom panel of Fig. 7(a) shows an overlap of the two asymmetries A_Y(UV1) for UV1 and A_Y(UV2) for UV2. If UV1 and UV2 were aligned perfectly, the asymmetries A_Y(UV1) and A_Y(UV2) would be totally symmetrical each other because geometry flip between UV1 and UV2 changes the spin polarization only. But a careful comparison between the two

asymmetries indicates that they are not totally symmetrical. This means that the geometry flip between UV1 and UV2 fails to remove the instrumental asymmetry completely using Eq. (24). Even so, the geometry flip using Eq. (24) is a very useful method to eliminate instrumental asymmetries involved.

The single statistical errors for Eqs. (17), (18) and (24) are given by

$$\begin{aligned}
\Delta A_Y &= \sqrt{\left(\frac{\partial A_Y}{\partial N_3(\mathrm{un})}\right)^2 (\Delta N_3(\mathrm{un}))^2 + \left(\frac{\partial \mathrm{A_Y}}{\partial \mathrm{N_4(un)}}\right)^2 (\Delta \mathrm{N_4(un)})^2} \\
&= \sqrt{\frac{4N_3(\mathrm{un})\mathrm{N_4(un)}}{\left(N_3(\mathrm{un}) + \mathrm{N_4(un)}\right)^3}}, \\
\Delta P_Y &= \sqrt{\left(\frac{\partial P_Y}{\partial A_Y}\right)^2 (\Delta A_Y)^2 + \left(\frac{\partial P_Y}{\partial A_Y^0}\right)^2 (\Delta A_Y^0)^2} \\
&= \frac{1}{S_{\mathrm{eff}}} \frac{(1-(A_Y^0)^2)}{(1-A_Y A_Y^0)^2} \Delta A_Y \\
&= \frac{1}{S_{\mathrm{eff}}} \frac{(1-(A_Y^0)^2)}{(1-A_Y A_Y^0)^2} \sqrt{\frac{4N_3(\mathrm{un})\mathrm{N_4(un)}}{\left(N_3(\mathrm{un}) + \mathrm{N_4(un)}\right)^3}}, \\
\Delta P_Y &= \sqrt{\sum_{\mathrm{i}=1,2} \left(\frac{\partial P_Y}{\partial N_3(\mathrm{UVi})}\right)^2 (\Delta N_3(\mathrm{UVi}))^2 + \sum_{\mathrm{i}=1,2} \left(\frac{\partial \mathrm{P_Y}}{\partial \mathrm{N_4(UVi)}}\right)^2 (\Delta \mathrm{N_4(UVi)})^2} \\
&= \frac{1}{S_{\mathrm{eff}}} \sqrt{\frac{4\sqrt{N_3(\mathrm{UV1})\mathrm{N_4(UV2)}}\sqrt{N_4(\mathrm{UV1})\mathrm{N_3(UV2)}}}{\left(\sqrt{N_3(\mathrm{UV1})\mathrm{N_4(UV2)}} + \sqrt{N_4(\mathrm{UV1})\mathrm{N_3(UV2)}}\right)^3}}.
\end{aligned} \tag{26}$$

C. Magnetic materials

In this subsection, we will show that the method developed above can be applied for the magnetic system in which an external magnetic field is applied. We present the spin resolved $2p$ core level photoemission spectra from thin film Fe, which are measured with circularly polarized light at the APS using the experimental setup shown in Fig. 4.

Under the experimental geometry given in Fig. 4, circularly polarized light (σ^+) hits the magnetic Fe thin film. The spin component P_Y is measured with a fixed helicity (σ^+) by applying external magnetic fields M^{up} parallel to the Y-direction and M^{down} antiparallel to the Y-direction. With M^{up}, we measure the counting rates $N_3(M^{\mathrm{up}})$ and $N_4(M^{\mathrm{up}})$, and

with $M^{\rm down}$, we measure the counting rates $N_3(M^{\rm down})$ and $N_4(M^{\rm down})$. Using these counting rates, Eq. (9) can be used to determine the spin polarization P_Y by substituting $Z \rightarrow Y$, $N_1(\sigma^+) \rightarrow N_3(M^{\rm up})$, $N_2(\sigma^+) \rightarrow N_4(M^{\rm up})$, $N_1(\sigma^-) \rightarrow N_3(M^{\rm down})$, $N_2(\sigma^-) \rightarrow N_4(M^{\rm down})$. P_Y can be written

$$P_Y = \frac{1}{S_{\rm eff}} \left(\frac{\sqrt{N_3(M^{\rm up})N_4(M^{\rm down})} - \sqrt{N_4(M^{\rm up})N_3(M^{\rm down})}}{\sqrt{N_3(M^{\rm up})N_4(M^{\rm down})} + \sqrt{N_4(M^{\rm up})N_3(M^{\rm down})}} \right). \tag{27}$$

From the Eq. (10) the instrumental asymmetry $A_Y^{\rm ins}$ can be written

$$A_Y^{\rm ins} = \frac{\sqrt{N_3(M^{\rm up})N_3(M^{\rm down})}}{\sqrt{N_4(M^{\rm up})N_4(M^{\rm down})}}. \tag{28}$$

Fig. 9 shows the spin resolved $2p$ spectra from the thin film Fe. In the bottom panel of Fig. 9 (a), according the Eq. (28), the instrumental asymmetry $A_Y^{\rm ins}$ is plotted as a function of kinetic energy. The $A_Y^{\rm ins}$ is fairly well constant over the entire energy range. The spin polarization P_Y is determined by the Eq. (27) and presented in the middle of Fig. 9 (a). It should be mentioned that the reason why the two magnetic fields $M^{\rm up}$ and $M^{\rm down}$ are needed in Eq. (27) is only to eliminated the instrumental asymmetry involved. If there were no instrumental asymmetry involved, a measurement with $M^{\rm up}$ would produce a spin polarization while a measurement with $M^{\rm down}$ would produce the identical spin polarization with opposite sign.

As shown in Fig. 9 (b) and (c), the spin polarization P_Y can also be determined with a magnetic field only using Eq. (18). Let us consider the case with $M^{\rm up}$ as shown in Fig. 9 (b). In the bottom panel of Fig. 9 (b) the asymmetry $A_Y = [N_3(M^{\rm up}) - N_4(M^{\rm up})]/[N_3(M^{\rm up}) + N_4(M^{\rm up})]$ is plotted as a function of kinetic energy. In order to use Eq. (18) a pure instrumental asymmetry A_Y^0 is assumed as shown in a line. The resulting spin polarization is shown in the middle panel of Fig. 9 (b). It is clear that this spin polarization is identical to the one determined with the Eq. (27). Similarly, the determination of the spin polarization with $M^{\rm down}$ only is shown Fig. 9 (c). The spin polarizations determined with $M^{\rm up}$ and $M^{\rm down}$ are identical, but they have reversed sign as expected. Fig. 9 shows that the spin polarization can be determined either by the Eq. (27) where two magnetic fields $M^{\rm up}$ and $M^{\rm down}$ are used to eliminate the instrumental asymmetry, or by Eq. (18) where a pure instrumental asymmetry A_Y^0 is assumed.

V. CONCLUSION

We have introduced a new method to eliminate the instrumental asymmetries in the spin resolved photoemission with unpolarized light. This new method is applied to extract the spin polarizations in the valence band and in the $4d$ core level photoemission from nonmagnetic Pt with unpolarized lights, as well as in the $2p$ core level photoemission from the magnetic Fe with circularly polarized light. It is concluded that this new methods can be used for the elimination of the instrumental asymmetries in the spin resolved photoemission with unpolarized and circularly polarized light from magnetic and nonmagnetic materials.

Finally, it is worth to note the following. We have extended the usual approach for the removal of instrumental asymmetry, from magnetization flipping to helicity flipping and even geometry flipping. In general, the magnetization flipping is the best behaved, with a constant instrumental asymmetry near 1.1. The helicity flipping and geometry flipping are not quite as well behaved, but still fall within acceptable behavior for spin analysis.

VI. ACKNOWLEDGMENTS

Lawrence Livermore National Laboratory is operated by Lawrence Livermore National Security, LLC, for the U.S. Department of Energy, National Nuclear Security Administration under Contract DE-AC52-07NA27344. This work was supported by the DOE Office of Basic Energy Science and Campaign 2/WCI/LLNL. The APS has been built and operated under funding from the Office of Basic Energy Science at DOE. We would like to thank the scientific and technical staff of Sector 4 of the Advanced Photon Source for their technical assistance in supporting this work.

---

[1] U. Heinzmann, Phys. Scr. **T17**, 77 (1987).

[2] U. Heinzmann and G. Schönhense, in *Polarized Electrons in Surface Physics*, edited by R. Feder (World Scientific, Singapore, 1985).

[3] J. Kirschner, *Polarized Electrons at Surfaces* (Springer, Berlin, Heidelberg, 1985).

[4] N. F. Mott, H. S. W. Massey, *The Theory of Atomic Collisions* (Clarendon Press, Oxford, 1965).

[5] J. Kessler, *Polarized Electrons*, 2nd ed. (Spring-Verlag, Berlin, 1985).

[6] D. M. Oro, W. H. Butler, F. C. Tang, G. K. Walters, and F. B. Dunning, Rev. Sci. Instrum. 62, 667 (1991).

[7] F.B. Dunning, Nucl. Instr. and Meth. in Phys. Res. A **347**, 152 (1994).

[8] G. C. Burnett, T. J. Monroe, and F. B. Dunning, Rev. Sci. Instrum. 65(6), 1893 (1994).

[9] G. Ghiringhelli, K. Larsson, and N. B. Brookes, Rev. Sci. Instrum. 70, 4225 (1999).

[10] U. Heinzmann, J. Phys. B **11**, 399 (1978).

[11] A. Gellrich, K. Jost, und J. Kessler, Rev. Sci. Instrum. **61**, 3399 (1990).

[12] S.-W. Yu and J. G. Tobin, Surface Science **601**, L127 (2007).

[13] S.-W. Yu and J. G. Tobin, Phys. Rev. B **77**, 193409 (2008).

[14] S.-W. Yu, T. Komesu, B. W. Chung, G. D. Waddill, S. A. Morton, and J. G. Tobin, Phys. Rev. B **73**, 075116 (2006).

[15] J. G. Tobin, S. A. Morton, S. W. Yu, G. D. Waddill, I. K. Schuller, and S. A. Chambers, J. Phys.: Condens. Matter **19**, 315218 (2007).

[16] T. Komesu, G. D. Waddill, S.-W. Yu, M. Butterfield, and J. G. Tobin, submitted to Phys. Rev. B, December 2008.

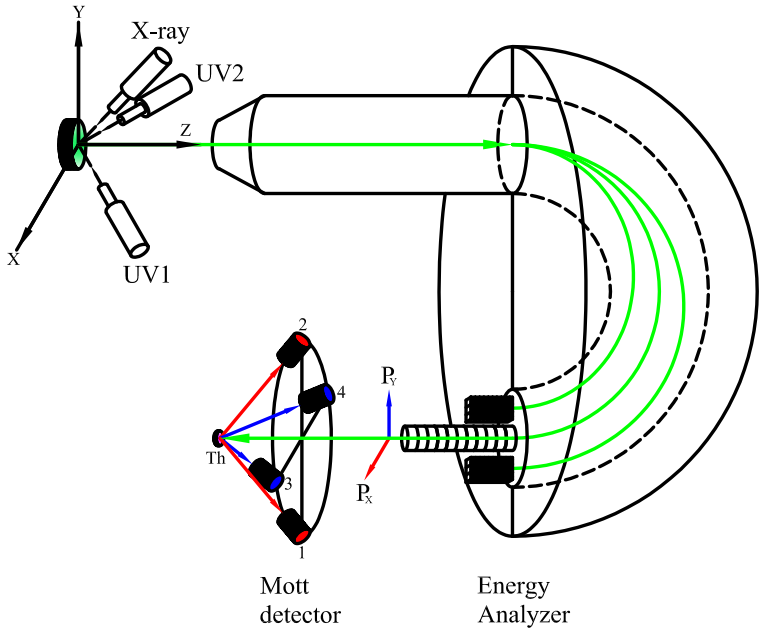

FIG. 1: (Color online) Sketch for the spin resolved photoemission spectroscopy at the Lawrence Livermore National Laboratory. There are two unpolarized UV sources (UV1 and UV2) in the X-Z plane and an unpolarized x-ray source in the Y-Z plane. The energies and the spins of the photoelectrons are analyzed by the hemispherical electron energy analyzer and the Mott detector, respectively. Two transversal spin components P_X and P_Y can be measured in Mott detector simultaneously.

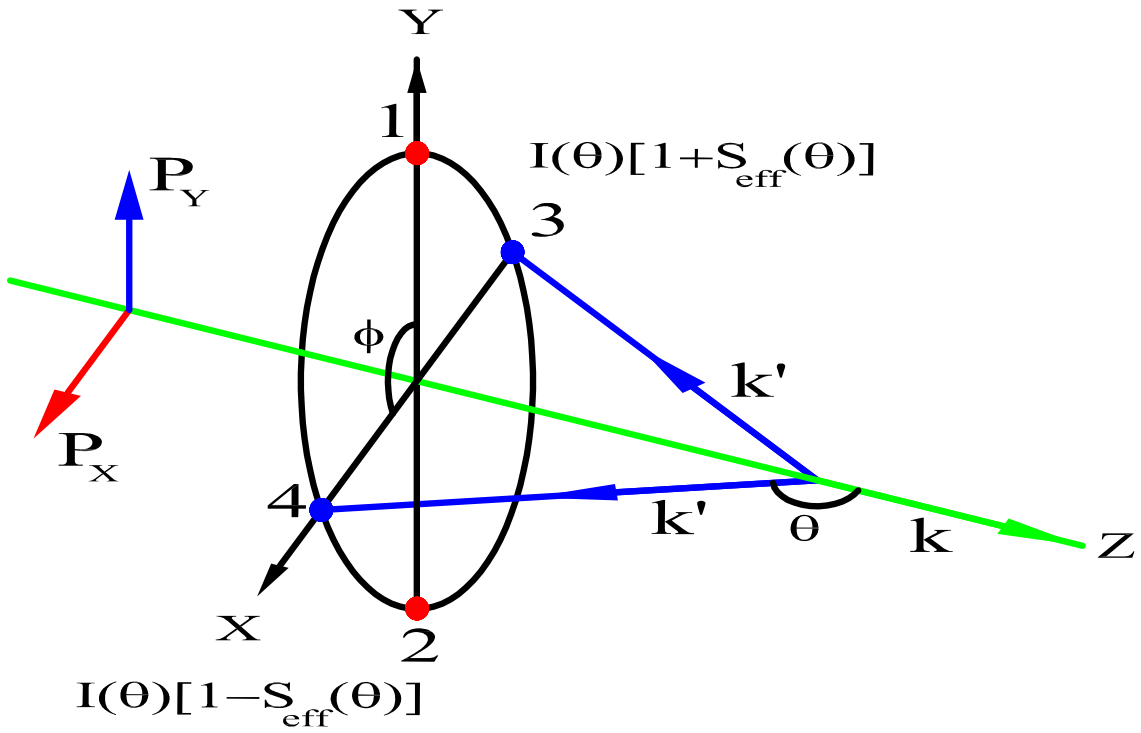

FIG. 2: (Color online) Left-right scattering asymmetry. An electron beam incoming along the Z-direction is back scattered at an scattering angle θ. According to Eq. (3), an electron beam polarized in the Y-direction results in maximum intensity $I(\theta)[1 + S_{\rm eff}(\theta)]$ at the counter 3 (left side) and minimum intensity $I(\theta)[1 - S_{\rm eff}(\theta)]$ at the counter 4 (right side). An electron beam polarized in the X-direction results in maximum intensity $I(\theta)[1 + S_{\rm eff}(\theta)]$ at the counter 1 (left side) and minimum intensity $I(\theta)[1 - S_{\rm eff}(\theta)]$ at the counter 2 (right side). Here, θ is the scattering angle (or polar angle) and ϕ is the azimuthal angle.

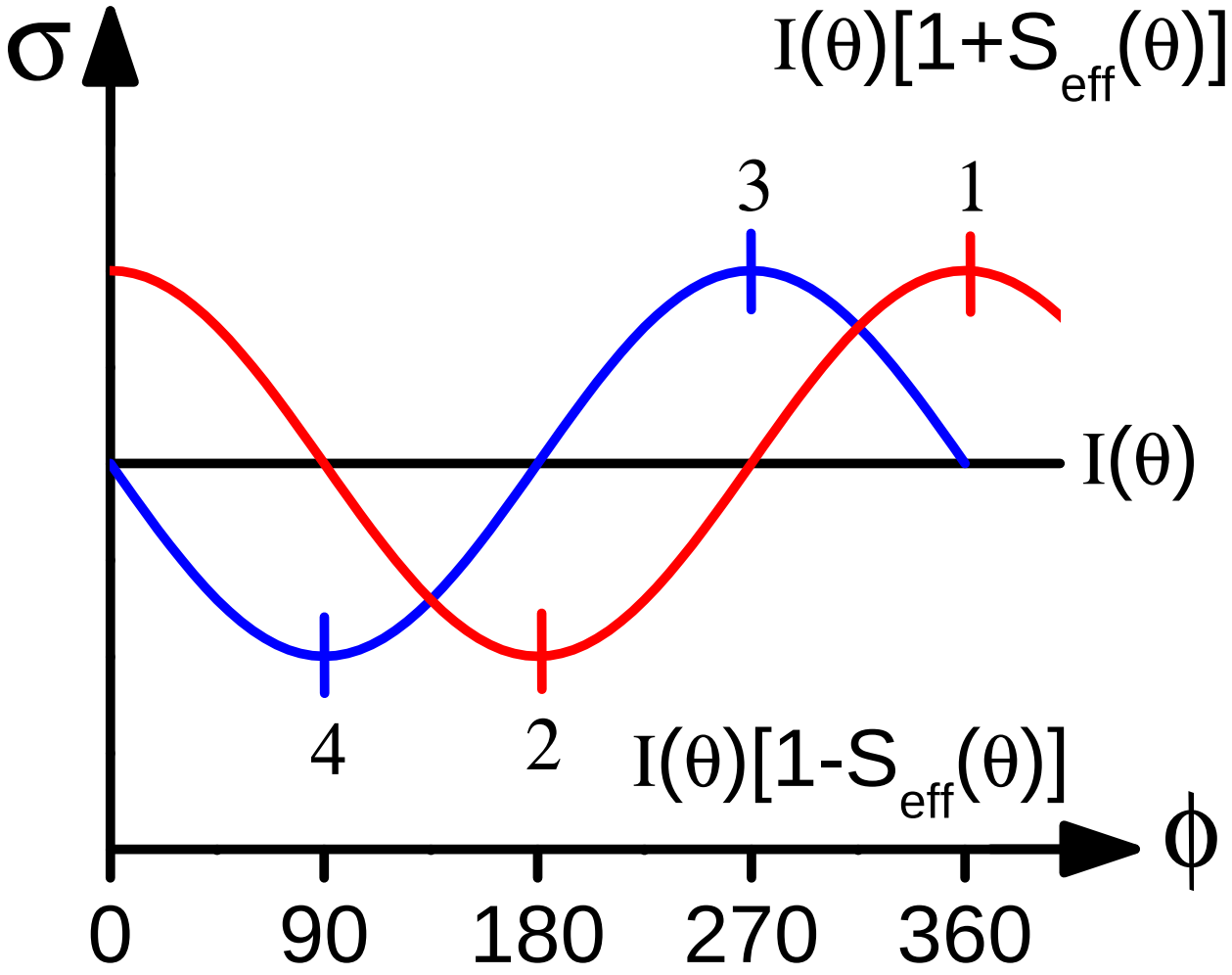

FIG. 3: (Color online) Azimuthal angle (ϕ) dependency of the scattering cross section $\sigma(\theta, \phi)$, according to the Eq. (3). It is worth noting that there would be no azimuthal angle dependency of the scattering cross section, $\sigma(\theta, \phi) = I(\theta)$ for all ϕ, if the effective Sherman function $S_{\text{eff}}(\theta)$ is zero.

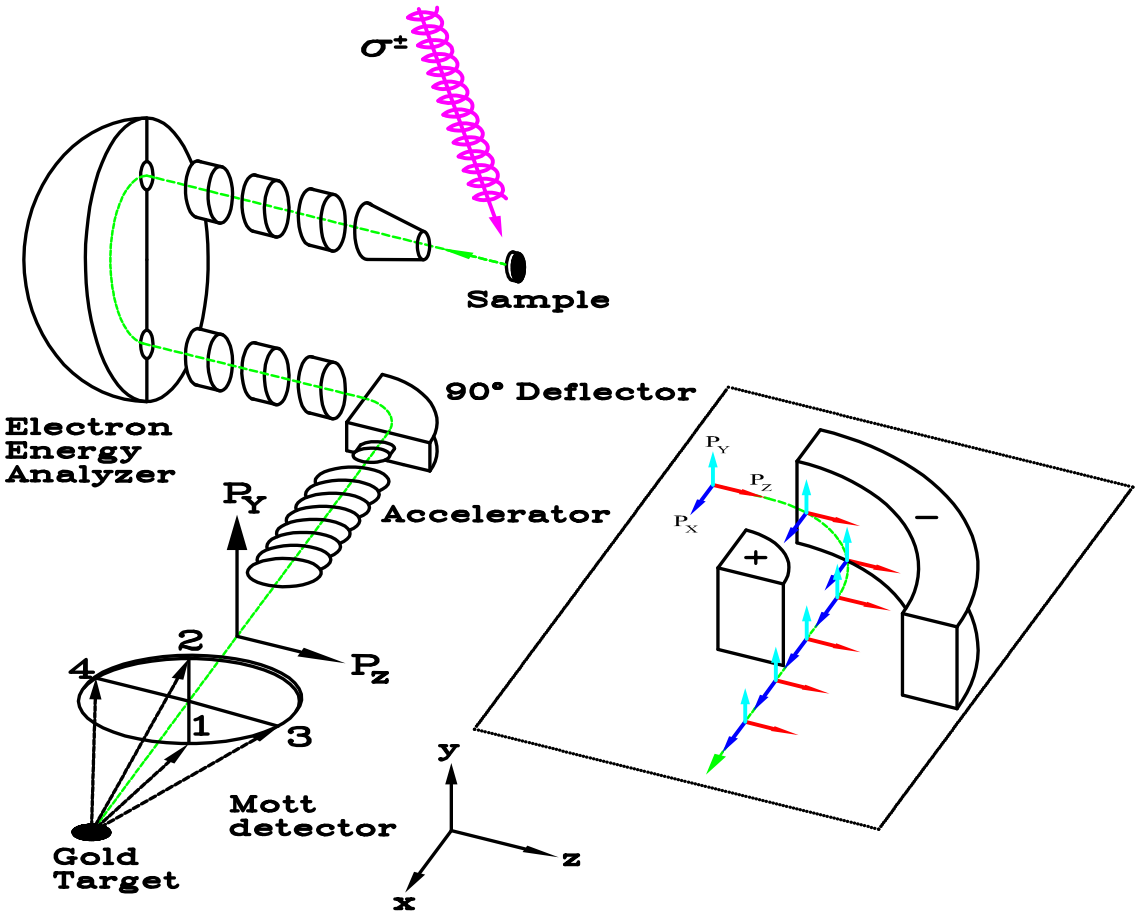

FIG. 4: (Color online) Sketch for the spin resolved photoemission spectroscopy at the Advanced Photon Source. Circularly polarized light creates the spin polarized photoelectrons. The energies of the photoelectrons are analyzed by the hemispherical energy analyzer. After that, the photoelectrons are deflected by 90° in an electrostatic deflector. After the deflection, the photoelectrons are accelerated with 25 keV into the Mott detector for their spin analysis. In the Mott detector, the two transversal spin components P_Y and P_Z can be measured. The role of the 90° deflector, which transfers a longitudinal component to a transversal component and vise versa, is shown in the inset. By passing the 90° deflector, the spin component P_Z is transformed from a longitudinal component to a transversal component while P_X is transformed from a transversal component to a longitudinal component. Therefore, P_X cannot be measured in the Mott detector. P_Y stays as a transversal component in this configuration.

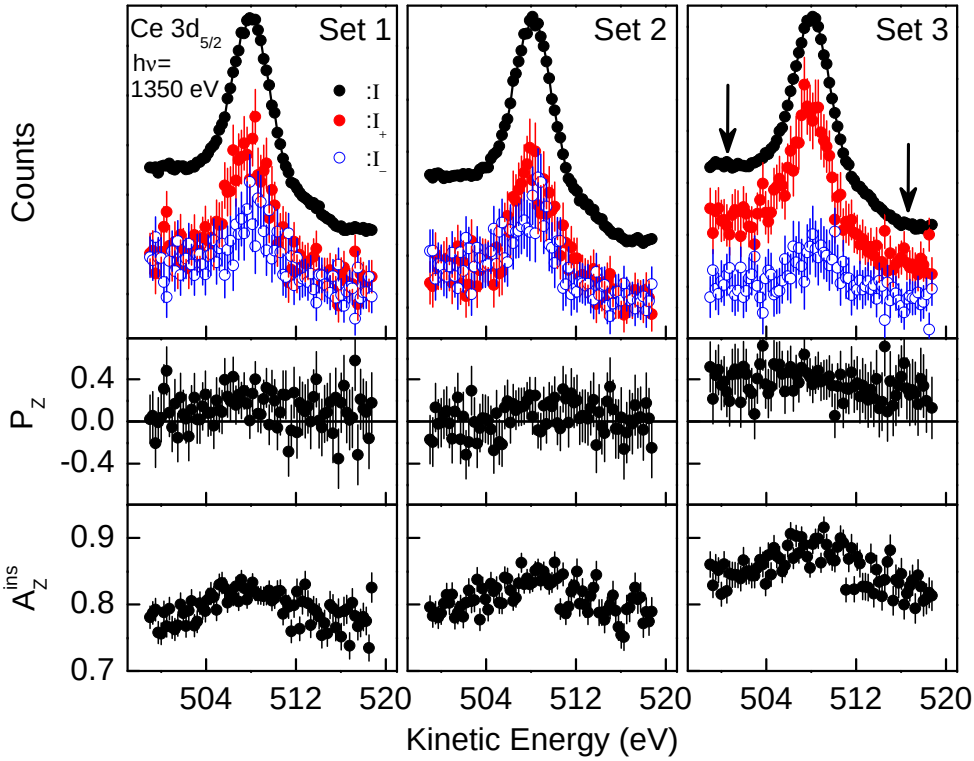

FIG. 5: (Color online) Spin resolved $3d_{5/2}$ photoelectron spectra of Ce generated with circularly polarized light of hν=1375 eV. Set 1, Set 2 and Set 3 are independent measurements in sequence. Top panels: I is the spin integrated total intensity while I_+ and I_- are the two spin separated partial intensities. I is separated into the partial intensities for spin parallel I_+ (antiparallel I_-) to the photon propagation direction, by means of $I_\pm = (I/2)(1 \pm P_Z)$. The vertical error bars $\Delta I_\pm$ given in I_+ and I_- represent the single statistical uncertainties included. They are calculated via $\Delta I_\pm = (I/2)\Delta P_Z$. Middle panels: electron spin polarization P_Z determined by Eq. (9). In determining the spin polarization, Eq. (9) is normalized by light polarization P_σ and $\cos 55°$ due to the 55° off-normal incidence of light and normal emission of electrons [14]. The vertical error bars given in P_Z represent the single statistic uncertainties determined by Eq. (11). Bottom panels: Instrumental asymmetry $A_Z^{\rm ins}$ determined by Eq. (10). The vertical error bars given in $A_Z^{\rm ins}$ represent the single statistic uncertainties determined by Eq. (11). The arrows marked on the outsides of the peak shown in the top panel of the Set 3 indicate the places where the large wrong spin polarizations appear due to the instrumental asymmetries which vary in time.

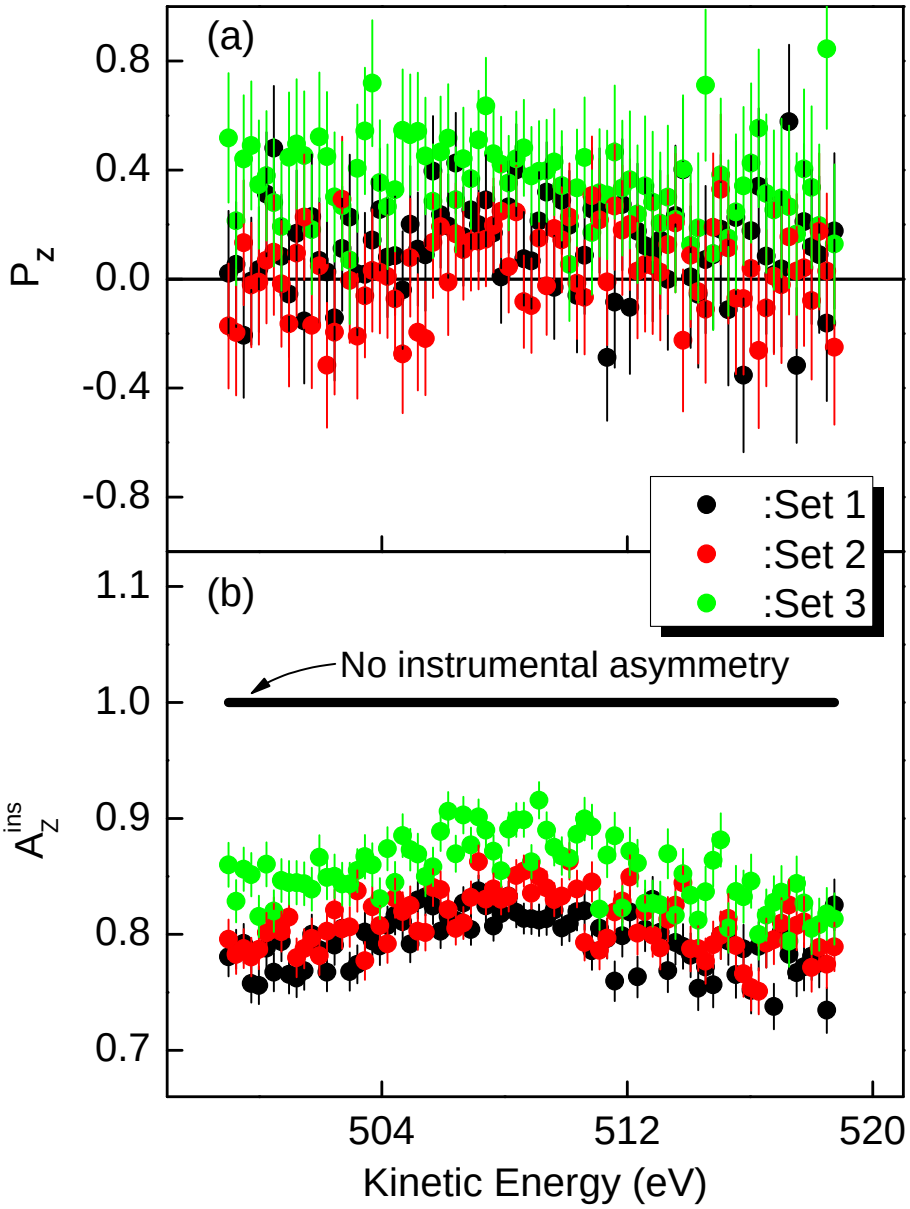

FIG. 6: (Color online) Comparison of the three independent measurements Set 1, Set 2 and Set3 measured in sequence. Upper panel is for the spin polarization P_Z and lower panel is for the instrumental asymmetry $A_Z^{\rm ins}$. Set 1 and Set 2 show a good agreement in $A_Z^{\rm ins}$, but Set 3 deviates from Set 1 and Set 2 significantly. The consequence is that the spin polarization for Set 3 differs from Set 1 and Set 2. The line in the lower panel shows $A_Z^{\rm ins} = 1$ where there is no instrumental asymmetry.

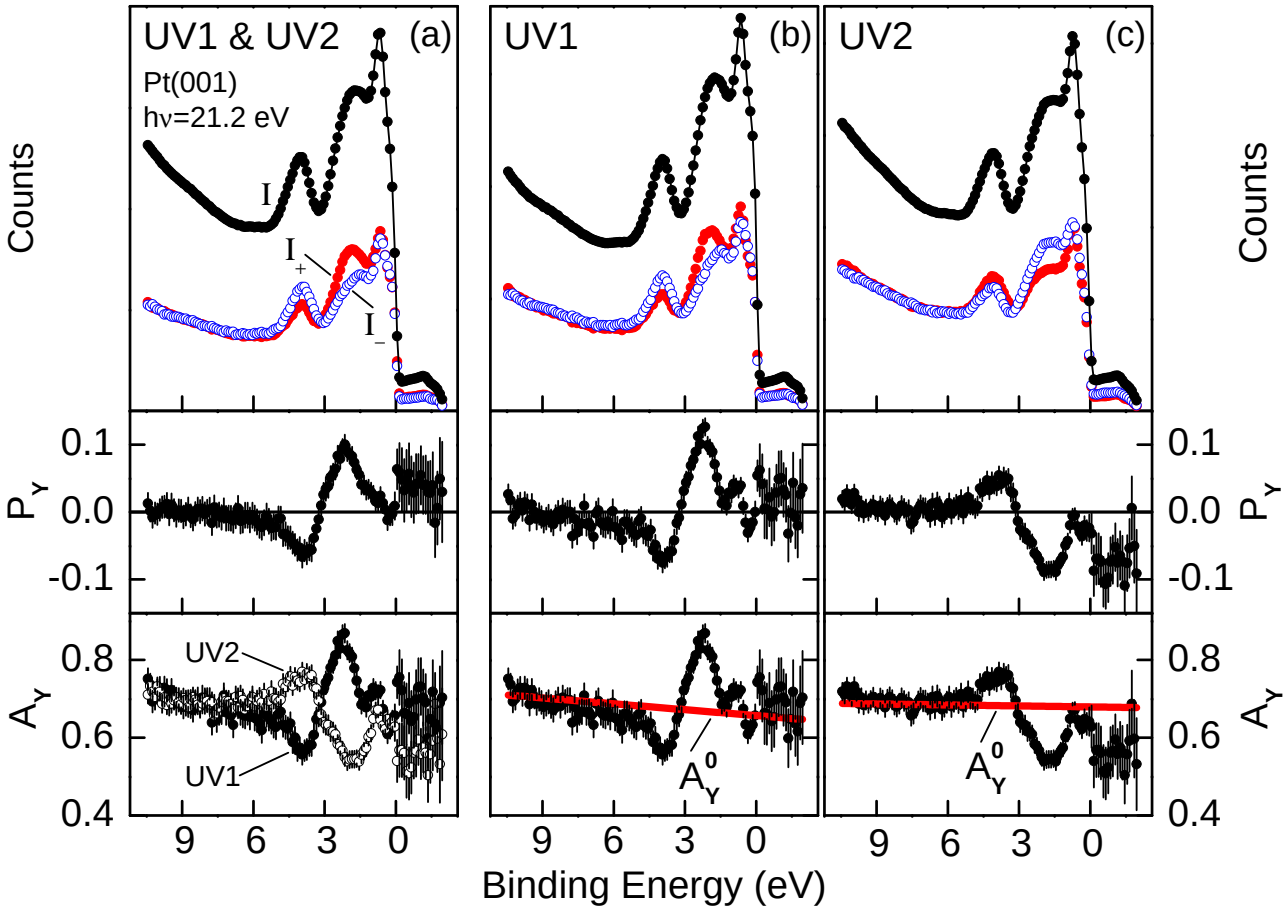

FIG. 7: (Color online) Determination of the spin polarization from the valence band photoemission of Pt(001) measured with unpolarized light of hν=21.2 eV. (a): Eq. (24) is used to determine P_Y. (b): Eq. (18) is used to determine P_Y for the measurement with UV1. The pure instrumental asymmetry A_Y^0 is assumed as a line shown in red in the bottom panel. (c): Eq. (18) is used to determine P_Y for the measurement with UV2. The pure instrumental asymmetry A_Y^0 is assumed as a line shown in red in the bottom panel. For (a)-(c), the error bars for A_Y and P_Y are given by Eq. (26). The spin integrated total intensity I is separated into the partial intensities for spin parallel I_+ (antiparallel I_-) to the Y-direction, by means of $I_\pm = (I/2)(1 \pm P_Y)$. For $I_\pm$, the error bars are not shown because they are smaller than the symbol size.

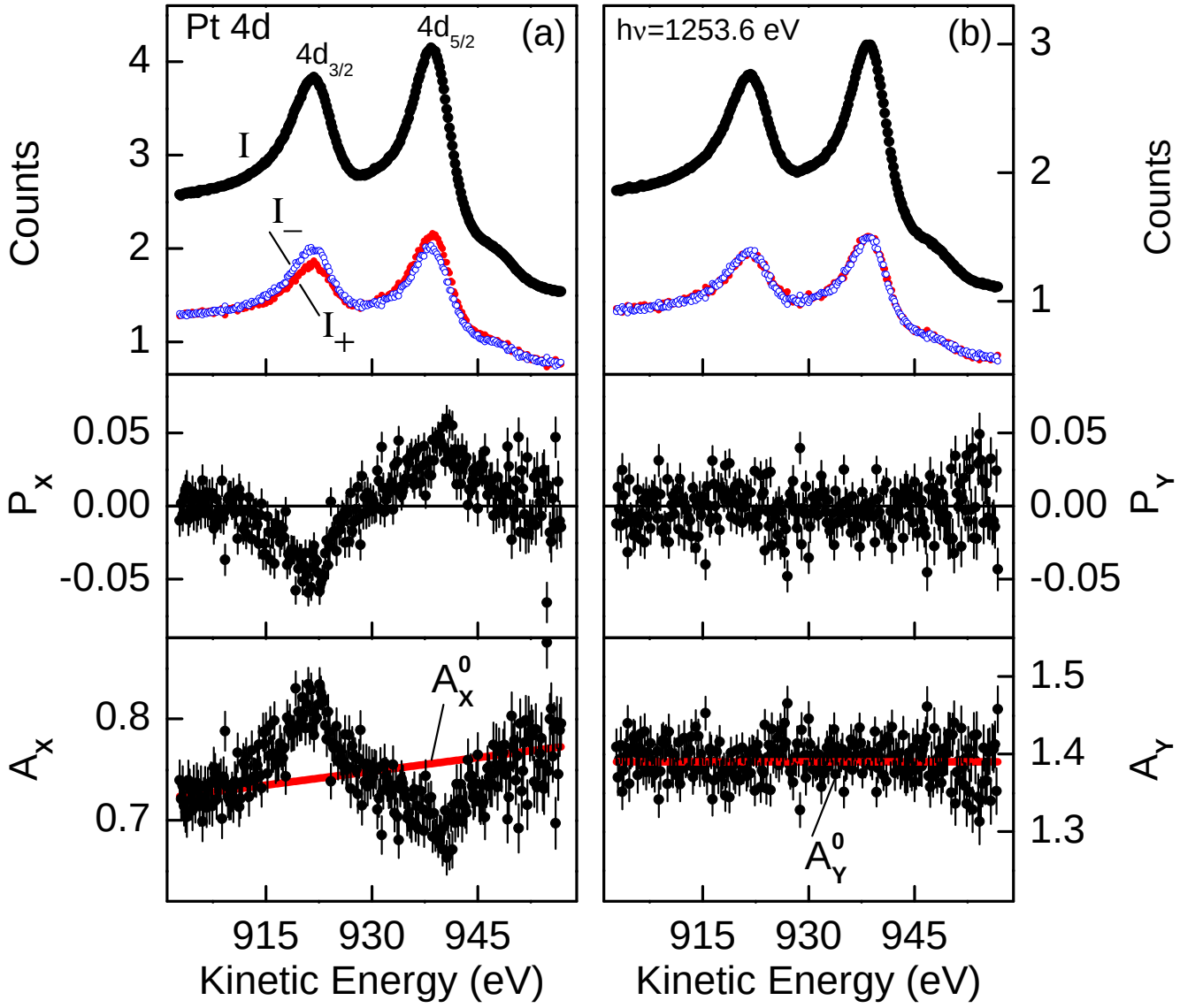

FIG. 8: (Color online) Determination of the spin polarization from the core level photoemission of Pt(001) measured with unpolarized x-ray of hν=1253.6 eV for the two spin components P_X in (a) and P_Y in (b). For (a) and (b), Eq. (18) is used to determine P_X and P_Y with assumed A_X^0 and A_Y^0. The error bars for A_X, A_Y and P_X, P_Y are given by Eq. (26). The spin integrated total intensity I is separated into the partial intensities for spin parallel I_+ and antiparallel I_- to X-direction for P_X (to Y-direction for P_Y), by means of $I_\pm = (I/2)(1 \pm P_{X(Y)})$. For $I_\pm$, the error bars are not shown because they are smaller than the symbol size.

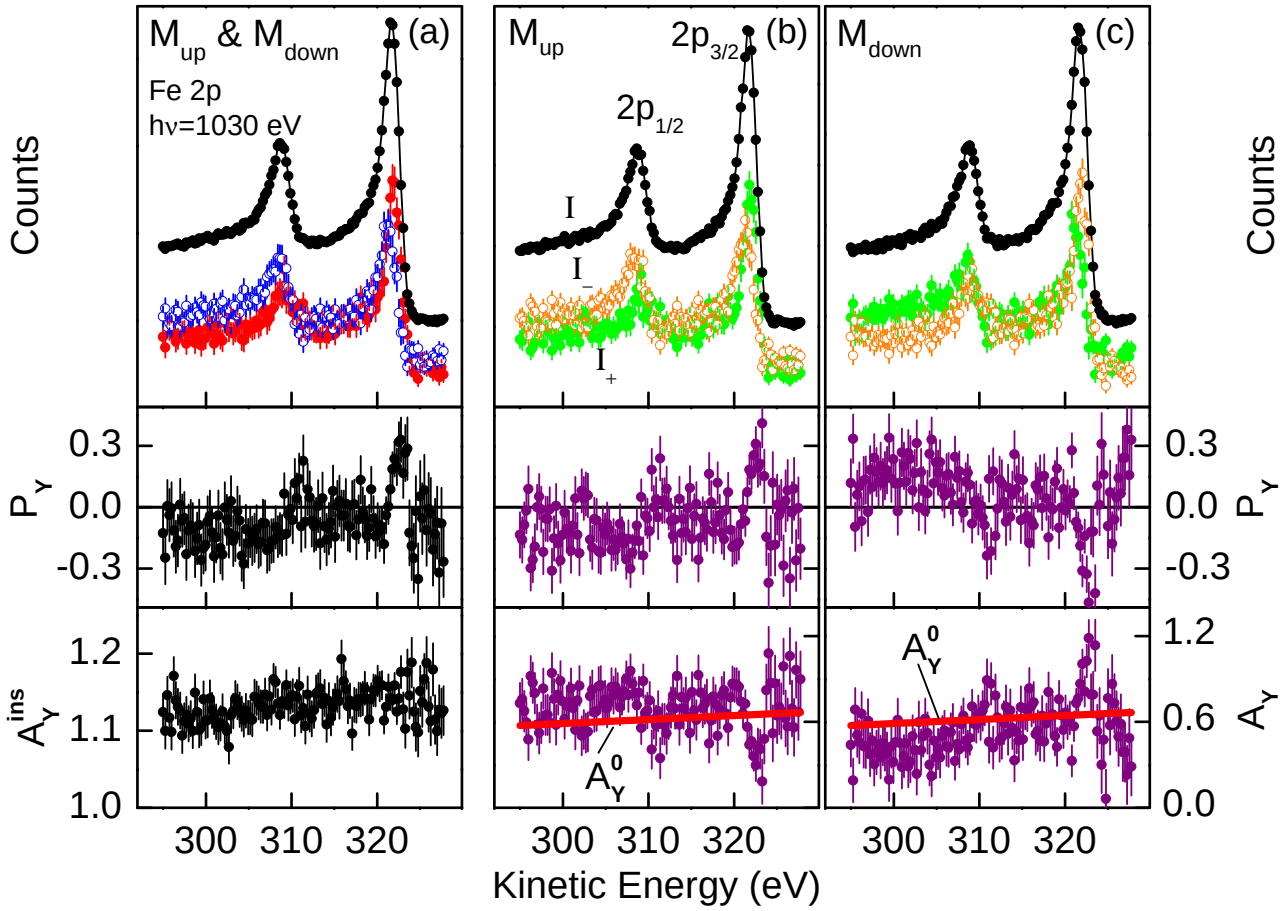

FIG. 9: (Color online) Determination of the spin polarization from the core level $2p$ photoemission of thin film Fe with circularly polarized light (σ^+) of hν=1030 eV using the two external magnetic fields $M^{\rm up}$ and $M^{\rm down}$. (a): spin polarization is determined using Eq. (27). (b) and (c): spin polarizations are determined using Eq. (18) with assumed A_Y^0. In determining the spin polarizations, Eq. (27) and Eq. (18) are normalized by light polarization P_σ [14]. For (a), the error bars $\Delta A_Y^{\rm ins}$ and ΔP_Y are given by Eq. (11). For (b) and (c), the error bars ΔA_Y and ΔP_Y are given by Eq. (26). For (a), (b), and (c), the spin integrated total intensity I is separated into the partial intensities for spin parallel I_+ and antiparallel I_- to Y-direction, by means of $I_\pm = (I/2)(1 \pm P_Y)$. The vertical error bars $\Delta I_\pm$ given in I_+ and I_- represent the single statistical uncertainties included. They are calculated via $\Delta I_\pm = (I/2)\Delta P_Y$.